Digital-Twins of composite aerostructures towards Structural Health Monitoring

Conference Paper · June 2021

DOI: 10.1109/MetroAeroSpace51421.2021.9511653

3 authors:

Dimitrios Milanoski
University of Patras
9 PUBLICATIONS **42** CITATIONS
SEE PROFILE

Georgios Galanopoulos
University of Patras
12 PUBLICATIONS **42** CITATIONS
SEE PROFILE

Theodoros Loutas
University of Patras
126 PUBLICATIONS **2,321** CITATIONS
SEE PROFILE

2021 IEEE 8th International Workshop on Metrology for AeroSpace
DOI: 10.1109/MetroAeroSpace51421.2021

Digital-Twins of composite aerostructures towards Structural Health Monitoring

Dimitrios P. Milanoski
Dept. of Mechanical Engineering & Aeronautics
University of Patras
Patras, Greece
d.milanoski@g.upatras.gr

Georgios K. Galanopoulos
Dept. of Mechanical Engineering & Aeronautics
University of Patras
Patras, Greece
g.galanopoulos@g.upatras.gr

Theodoros H. Loutas
Dept. of Mechanical Engineering & Aeronautics
University of Patras
Patras, Greece
thloutas@upatras.gr

***Abstract*—The present work is primarily dedicated to the development and validation of a Digital Twin representative of an aeronautical structure. A finite element model is thus created to simulate the structural response of a composite single-stringer panel under compressive loading. Quasi-static tests are conducted and health monitoring techniques, i.e. displacement and strain measurements via digital image correlation and fiber Bragg grating sensors respectively, are utilized. The mechanical response of the model presents very good agreement with the experimental evidence. The validated model is then exploited, augmented by exogenous details, i.e. external loading, to train a surrogate mathematical model. The resultant surrogate maps efficiently the Digital Twin strains with respect to the load. This advantage is envisaged by the Digital-Twin concept where real-time data flowing from the physical twin would be used to detect the presence of skin-to-stringer disbonds. The proposed methodology is tested for the case of an artificially disbonded panel, subjected to block loading compression-compression fatigue, utilizing static strains periodically acquired during several quasi-static test intervals.**

***Keywords*—Digital Twin, Composite structures, Fiber Bragg grating sensors, Surrogate modeling, Structural Health Monitoring, Damage diagnosis**

I. Introduction

The *Digital-Twin* (DT) concept was initially introduced the previous decade [1], [2], [3], [4] in an attempt to reevaluate the way that complex physical systems and computational models may coalesce, towards novel decision making [5], [6]. The DT paradigm combines high-fidelity numerical models updated by an influx of data coming from the real world, i.e. the physical twin, in order to mirror the health condition of the structure as well as perform predictions regarding its remaining useful life [7], [8], [9]. The concept is currently adopted by several industrial sectors besides astronautics and aeronautics [10]. However, a unified mathematical formalism of DTs was absent, and authors in [11], [12] provided the ingredients to achieve this. In their papers, important aspects are detailed, such as the importance of validation of the DTs or the context in which a DT is capable of generalizing its response. Supplementary, the advent of machine learning enabled new possibilities for the aspect of merging an existing DT [13], [14], or generally a validated model, with data flowing from its physical counterpart [15], [16]. Hence, model-based Structural Health Monitoring (SHM) methodologies emerged [17], [18], [19] enabling monitoring of complex structures and phenomena like fatigue damage development [20], [21], [22].

This paper is mainly oriented towards validating a FE model - DT [23] within a context of interest. For that purpose, experimental evidence is provided to verify the response of the model which will in the future be used to train a black-box surrogate model enhanced with environmental- and damage-related information. In Section II the physical and digital twins are presented. Section III shows the experimental procedure and the verification of the DT. In the last Section IV, the development of a DT-substitute surrogate model is discussed. In the end, we propose a fatigue damage growth monitoring methodology based on the surrogate model response which will be blended with response data acquired by a variable-amplitude fatigue test campaign [24].

The work was financially supported by the European Union's Horizon 2020 research and innovation programme ReMAP (Grant Agreement Number: 769288)

II. Digital Twin Development

A. Context and target output

In the current section, the main context in which the DT operates will be defined. It is of great importance to clarify that a DT does not abstractly generalize its response under unseen conditions [11]. Hence, we seek to consolidate a model that will be reflecting the response of its physical counterpart. In the present work, a composite single-stringer panel is considered which is subjected to a quasi-static (QS) compressive load. The composite panel was manufactured by OPTIMAL Structural Solutions Lda (Portugal). The specimen consists of a flat skin and a centrally-placed T-section stringer, both made of graphite/epoxy IM7/8552 prepregs. The flat skin consists of 14 plies with a stacking sequence [45/-45/0/45/90/-45/0]s whilst the stringer's flange is composed by a 10-layer lamination [45/-45/0/-45/45]s. The stringer's web is formed by doubling the latter plies.

We envisage a model/DT-based SHM methodology that utilizes strain components from the specimen's surface. Thus, the target output $\boldsymbol{y}$ of the model $\mathcal{M}$, would be the equivalent strain component of the continuum medium.

$$\mathcal{M}(\boldsymbol{\mathcal{X}}) = \boldsymbol{y} \tag{1}$$

where, $\boldsymbol{\mathcal{X}}$ generally refers to the model variables, e.g. Cartesian coordinate, magnitude of external forces etc. The mathematical model yielding $\boldsymbol{y}$ is generally expressed by the following set of governing equations of linear elasticity [25]:

- Equations of motion (Newton's 2nd law):

$$\boldsymbol{\nabla} \cdot \boldsymbol{\sigma} + \bar{\boldsymbol{F}} = \rho \ddot{\boldsymbol{u}} \tag{2}$$

- Strain-displacement equations:

$$\boldsymbol{\varepsilon} = \frac{1}{2}(\boldsymbol{\nabla u} + \boldsymbol{\nabla u^T}) \tag{3}$$

- Constitutive equations (Hooke's law):

$$\boldsymbol{\sigma} = \mathbb{C} : \boldsymbol{\varepsilon} \tag{4}$$

where, ρ is the material density, $\bar{\boldsymbol{F}}$, $\boldsymbol{u}$ designate the vectors of the body forces per unit volume and the displacements respectively, $\boldsymbol{\sigma}$, $\boldsymbol{\varepsilon}$ are the (Cauchy) stress and strain second-order tensors respectively and $\mathbb{C}$ refers to the fourth-order stiffness tensor. In the absence of inertia phenomena (2) is transformed to equilibrium equations. The solution of the mathematical model is obtained by solving the weak formulation of (2)-(4) with the finite element method (FEM).

B. Finite element model

As priorly mentioned, the determination of $\boldsymbol{\sigma}$, $\boldsymbol{\varepsilon}$, and $\boldsymbol{u}$ fields is numerically obtained by using a FE model. For that purpose, ABAQUS/STANDARD™ commercial FE package was used. The simulation of the macroscopic response consists of two parts; first, a linear buckling analysis obtains the system eigenvalues and the corresponding (buckling) mode shapes. Secondly, the latter are introduced to the non-linear analysis as initial imperfections, facilitating the buckling of the overall panel. Here, only the first mode shape is used with a selected amplitude of 5% of the skin's thickness. An earlier version of the model is presented in our preceded paper [23]. In the present work the FE model is updated and finely tuned; both skin and stringer are now modeled using reduced-integration continuum shell elements (SC8R). An approximate global mesh size of 1.25 *mm* is used with three elements through the thickness of each member of the panel. The cast-tabs of the panel are explicitly designed using general purpose three-dimensional brick elements (C3D8R) with a 4.00 *mm* global mesh size. The cast-tabs are made of an epoxy resin AXSON® EPO 5019 (E=6000 MPa, ν=0.3). The ply properties used are presented Table I. Intralaminar damage is omitted for the current analysis. Finally, the equilibrium is iteratively solved using the Newton-Raphson solver incorporating large displacement formulation. In Fig. 1 the FE model-DT is depicted, accompanied by its physical counterpart.

TABLE I: PLY PROPERTIES OF IM7/8552

E_{11} [MPa]	$E_{22} = E_{33}$ [MPa]	$\nu_{12} = \nu_{13}$ [−]	ν_{23} [−]	$G_{12} = G_{13}$ [MPa]	G_{23} [MPa]
161000	11380	0.32	0.45	5290	3900

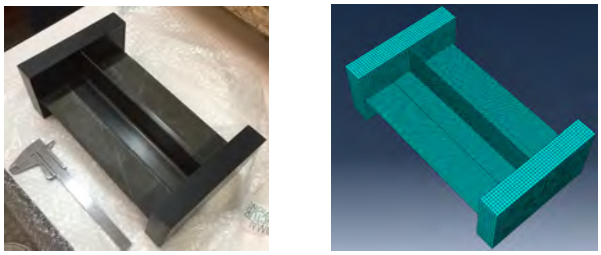

Fig. 1: Specimen (left) and DT (right) depiction.

III. EXPERIMENTAL VALIDATION OF THE FE MODEL

A. Quasi-static compression test

The composite single-stringer panel is subjected to QS compression upon failure. Displacement control boundary conditions (BCs) are applied, with a 0.5 *mm/min* rate. In total, two specimens were tested in the facilities of Applied Mechanics Lab. For that purpose, a servohydraulic INSTRON 8802 test machine with load capacity ± 250 *kN* was utilized. One linear variable differential transformer (LVDT) instrument was properly fixed upon the tabs in order to capture the actual shortening of the panel. The initial linear response of the panels ended at approximately a region amidst 16.5-18.0 *kN* when buckling initiated. Specimens L1-08 and L1-10 withstood a total load of 95.6 and 99.3 *kN* respectively, prior to collapsing. Force-shortening curves obtained by the test are plotted against the numerical elastic analysis predictions in Fig. 2.

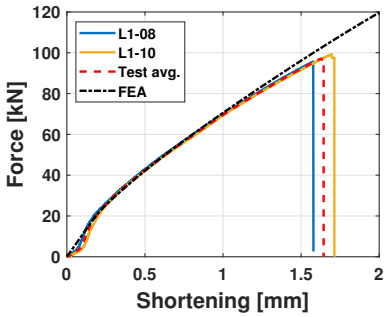

Fig. 2: Experimental and numerical force - shortening curves.

B. Digital Image Correlation measurements

Initiation of buckling was not able to be identified by eyesight. However, Digital Image Correlation (DIC) displacement measurements captured the initiation point of buckling, characterized by a jump on the out-of-plane displacements at

the skin surface. DIC measurements have only been taken for specimen L1-08. The specimen was painted (speckle pattern) from the back side of its flat skin. A comparison between the displacements of FEM and DIC is also provided in Fig. 3. The software ARAMIS (GOM MBH) was used to extract the DIC measurements.

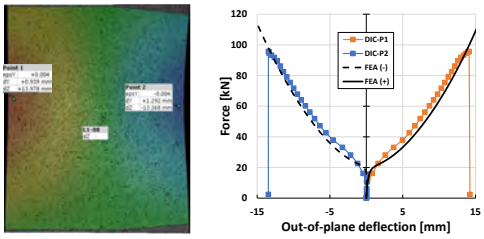

Fig. 3: Out-of-plane displacement field contour measured with DIC (left) and comparison with FE model (right).

C. Strain sensing via fiber Bragg grating sensors

Strain sensing was achieved using a fiber-optic sensor (FOS) with Bragg gratings (FBGs) [26], [27]. More specifically, a commercial sensor tape was provided by SMARTEC S.A. (Switzerland). The tapes were mounted on the stringer feet with a GRILTEX® copolyimide adhesive. A fully sensorized specimen is depicted in Fig. 4. Piezoelectric (PZT) and acoustic emission (AE) sensor data are not included in the current work. Each FOS contains five FBGs along its length with a 30-*mm* spacing between consecutive sensors. In every specimen, the central FBG was approximately placed at the center of the total span of the foot. Strain acquisition was achieved with a 2-channel MICRON OPTICS INC. SM130. Indicatively, in Fig. 5 we present the readings of three FBGs accompanied by the strains received by the FE model in the corresponding regions.

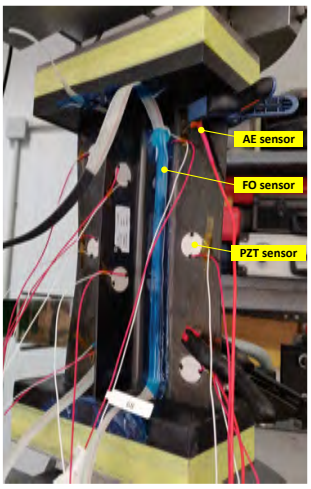

Fig. 4: Sensorized specimen.

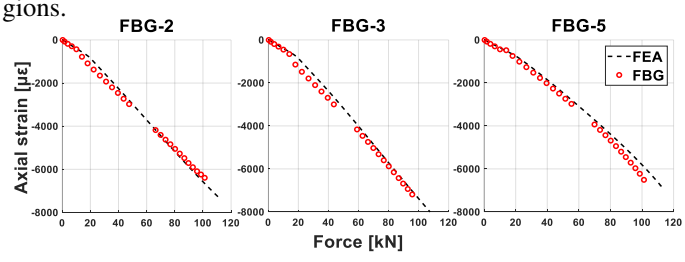

Fig. 5: Experimentally and numerically obtained strain readings.

IV. DT-Based Damage Diagnosis Concept

A. Pristine baseline damage diagnosis

In the following, we focus on combining the validated DT predictions with sensor data acquired during experiments on the physical twin for diagnostic purposes. Generally, diagnostic SHM tasks are separated into hierarchical levels that encompass the detailed characterization of damage. More specifically, each level attempts to determine the following: Level - 1) damage- presence, 2) localization and 3) quantification. The proposed methodology provides evidence regarding the first two levels based on the exploitation of a DT representing the pristine specimen. Thus, a reference baseline is defined, and the DT's output will be compared to experimental ones acquired from permanently affixed FBGs along the panel's foot. Intuitively, the longitudinal strains of the DT should only be correlated with experimental ones under the same load. Thus, the load is a constraint of the model which needs to be properly defined before any strain correlation as the following strain-based Health Indicator (HI) dictates:

$$\mathrm{HI}_i = \left| \frac{\varepsilon_{ref}^{(i)} - \varepsilon_t^{(i)}}{\varepsilon_{ref}^{(i)}} \right| \tag{5}$$

where $i = 1,\ldots,10$ denotes the i-th FBG sensor, $\varepsilon_{ref}^{(i)}$ represents the reference, i.e. DT's longitudinal strain and $\varepsilon_t^{(i)}$ the experimentally acquired strain at some random time during test.

The rationale behind this methodology lies on the fact that typical damages of composite materials, as interfacial delamination are, disturb the strain field at the adjacent region of the damage [23], [28], [29]. This effect is clearly intensified when the panel is in the post-buckling regime. Indicatively, Fig. 6 depicts the distributions along the two stringer feet, provided by a FE model incorporating a 30x30 mm^2 skin-to-stringer disbond. It is evident that the strain is intensified in the proximity of the disbond edges. Also, despite the local nature of the strain modification, as the load increases, we can also observe divergence from the pristine distribution at remote regions like the center of the panel. On the other hand, negligible deviation between pristine and disbonded states is observed along the bonded foot.

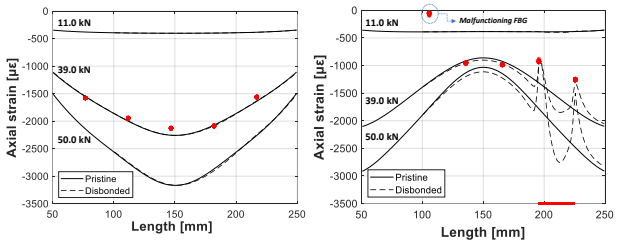

Fig. 6: Numerical strain distributions for pristine and disbonded panel: bonded (left) and disbonded (right) foot. The red scatter points ($*$) indicate experimental strains from an artificially disbonded panel [24].

B. Surrogate modeling

Generally, damage diagnosis lacks a well-posed definition of the inverse problem. Someone needs to possess *a priori* knowledge regarding the damage parameter with respect to the target output. Such a demand frequently becomes impractical as an *in-situ* estimation of such information is impossible during operational conditions. Hence, a robust approach is to utilize a surrogate model which maps the output of the DT in the multidimensional space of the state vector $\boldsymbol{\mathcal{X}}$. We can freely add as many variables within the state vector, for example, a damage variable that specifies the delaminated area of an interfacial disbond amidst skin/stringer or environmentally-related variables such as BCs, e.g. load magnitude. In the current methodology, we utilize a pristine DT, thus damage-related information will be absent. Thus, $\boldsymbol{\mathcal{X}} = \left\{\boldsymbol{x}^{(i)}, \boldsymbol{z}^{(i)}, \boldsymbol{P}^{(i)}\right\}_{i=1}^{N}$, where $x^{(i)}, z^{(i)}$ refer to the FBGs coordinates at their relevant locations and P refers to the load magnitude acting on the specimen. Hence, we follow a supervised learning approach based on Radial Basis Function (RBF) models [30]. We consider totally N input/output combinations, $\left\{\boldsymbol{\mathcal{X}}^{(i)}; \boldsymbol{y}^{(i)}\right\}$, acquired from the DT's FE model. The surrogate model obeys the following interpolation condition, for a parametric or fixed basis function ψ:

$$\widetilde{\mathcal{M}}(\boldsymbol{\mathcal{X}}^{(j)}) = \sum_{i=1}^{N} w_i \psi(||\boldsymbol{\mathcal{X}}^{(j)} - \boldsymbol{c}^{(i)}||) = \boldsymbol{y}^{(j)} \tag{6}$$

The abovementioned expression is conveniently simplified when the basis centers coincide with the data points, i.e. $\boldsymbol{c}^{(i)} = \boldsymbol{\mathcal{X}}^{(i)}$, leading to:

$$\boldsymbol{\Psi w} = \boldsymbol{y} \Leftrightarrow \boldsymbol{w} = \boldsymbol{\Psi}^{-1}\boldsymbol{y} \tag{7}$$

where, $\boldsymbol{\Psi}_{i,j} = \psi(||\boldsymbol{\mathcal{X}}^{(j)} - \boldsymbol{\mathcal{X}}^{(i)}||)$, is the so-called Gram square matrix. For our case we have selected a fixed basis function, namely a cubic $\psi(\rho) = \rho^3$. The particular surrogate model was cheap to evaluate its response, i.e. longitudinal strain, at the relevant regions where the FBGs were placed. Totally, 100 loads within the range [0,70] *kN* have been used for training purposes; 50% of the training data were used for cross-validation purposes, yielding a RMSE for the cross-validation set equal to 1.21 $\mu\varepsilon$. Note that all variables, including the output one, have been normalized in the range [0,1]. The advantage of possessing such a trained model is associated to its prompt availability during operation of the physical-twin. Prior to proceeding at the strain correlation between the DT and experimental measurements, we shall identify and validate the load acting on the structure, at every measuring instance *t*. Based on the observations of Section IV.A, we exploit the insignificant strain modification along the bonded foot. The load will be determined from a sensor, or group of them, whose strains will be correlated with those of the DT's. By selecting a reference sensor at a remote (unaffected by damage) location $(x^{(r)}, z^{(r)})$, the load P will be determined by minimizing the following squared ℓ^2-norm objective function F:

$$P = \underset{P}{\operatorname{argmin}}\, F(x^{(r)}, z^{(r)}, P) = \underset{P}{\operatorname{argmin}} \left\{||\widetilde{\mathcal{M}}(x^{(r)}, z^{(r)}, P) - \boldsymbol{y}^m||^2\right\} \tag{8}$$

where $\boldsymbol{y}^m$ is an experimentally measured strain value from the reference FBG at instance *t*. The load is then iteratively estimated utilizing the steepest (gradient) descent method:

$$P_{n+1} = P_n - \gamma \frac{\partial F}{\partial P} \tag{9}$$

with step size γ. The derivative term of the objective function is numerically computed using central differences:

$$\frac{\partial F}{\partial P} = \frac{1}{\epsilon}\left[\widetilde{\mathcal{M}}(x, z, P) - \boldsymbol{y}^m\right] \cdot \left[\widetilde{\mathcal{M}}(x, z, P + \epsilon) - \widetilde{\mathcal{M}}(x, z, P - \epsilon)\right] \tag{10}$$

where ϵ is a small perturbation, e.g. $\epsilon = 10^{-4}$.

C. Fatigue test and results

The overall SHM methodology is schematically depicted in Fig. 7. The methodology was evaluated for a specimen that contained an artificially-induced 30x30 mm^2 disbond as shown in Fig. 8. The specimen was subjected to block compression-compression fatigue excitation [24]. Every 500 cycles a QS test interval was conducted, during which experimental static strains were recorded. The QS test was conducted within maximum limit of fatigue at the relevant period, i.e. [0.5,Pmax] *kN*. The algorithm was evaluated utilizing the maximum compressive strain per QS test. This lies on the observation that the strain modification is intensified as the load increases.

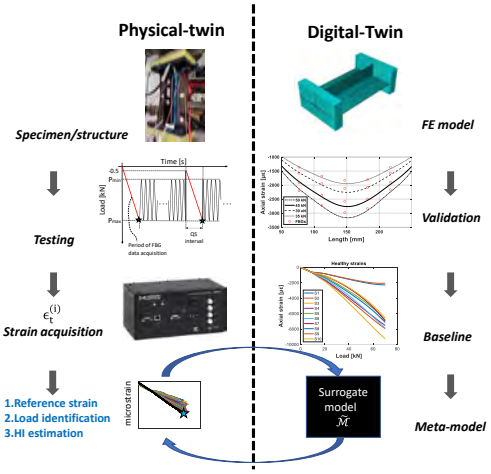

Fig. 7: Overall DT-based SHM methodology.

The FBGs of the bonded foot, namely FBG 6-10, were tested as potential load evaluators. FBG-9 derived the lower error between the actual load from the rest of the sensors affixed at the bonded foot. Results only from this FBG will be presented. Fig. 9 presents the load predictions of the algorithm. Random initialization of the load was also incorporated within the range [0,70] *kN*. A proper step size γ was investigated via trial and error to prevent overshooting of the iterative solution. After having defined the load at each measurement instance

t, the HI is calculated for every FBG sensor. Intuitively, the HI shows approximately zero value (based on the tolerance of the gradient descent) at the reference sensor, as a result of the minimization between the experimental and DT's strain of the said sensor. The evolution of every HI is presented in Fig. 10. An *ad hoc* threshold was selected to detect the damage-affected sensors. The value represents an average error between an array of FBG strain measurements, acquired during the first 60 QS tests, with those derived from an equivalent disbonded FE model. During those tests, it was indirectly validated, via *in-situ* non-destructive (NDT) measurements with a DolphiCam, that the nominal disbond did not propagate [24]. The threshold is set equal to 0.06.

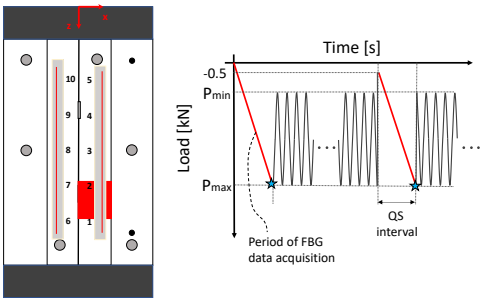

Fig. 8: Schematic of the disbonded specimen accompanied by the location of the FBGs (left) and test plan preview (right).

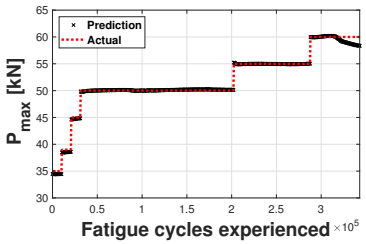

Fig. 9: Performance of the load-identification algorithm using FBG-9 as reference sensor.

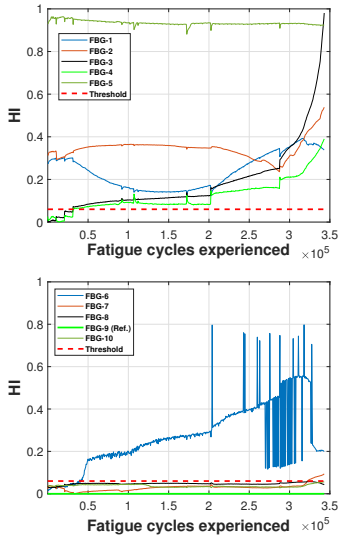

Fig. 10: HIs of disbonded (top) and bonded (bottom) foot.

V. Conclusion

Initially, the deterministic load identification approach presents a robust behavior for an extended period of $345k$ fatigue cycles till catastrophic failure of the panel. Utilization of a damage-unaffected sensor as load evaluator was efficiently achieved. The maximum estimated error on the load prediction (related to one of the reference sensors 7,8,9 or 10) is presented in Table II for every block of fatigue. Hence, the forthcoming valid estimation of the HIs allowed the prediction of damage presence, in the proximity of FBG-1 and FBG-2. The HI values of these sensors presented higher values than the threshold throughout the test span. Also, we identify a sensor, namely FBG-5, that has possibly lost adequate adhesion at its region, resulting in negligible readings throughout the duration of the test. It is evident that prior to the propagation of the nominal disbond, FBG-3, and FBG-4 present values lower than the threshold. However, as the maximum load increases in combination with disbond propagation, they gradually increase their values associating thus with the increasing degradation of the test article. On the other hand, it is worth noting that HI on FBGs 7-10 remained during the whole period below the threshold value, preventing a false alarm. From the bonded foot, only FBG-6 showed an increasing trend. As propagation of the disbond along the width of the flange was not observed, via NDT measurements, we deduce that it might have partially lost adequate adhesion to the specimen. The authors are currently dedicated on enhancing this methodology using a surrogate model augmented by damage-related variables.

TABLE II: Aggregated data regarding the performance of the load identification algorithm

$P_{\max}$ [kN]	Max. prediction error [%]	Fatigue cycles experienced [-]	Disbond propagation [Y/N]
35.0	4.01	10,000	N
39.0	4.02	10,000	N
45.0	4.16	10,000	N
50.0	4.03	170,000	Y
55.0	3.59	85,000	Y
60.0	10.08	60,000	Y

Acknowledgment

The authors would like to acknowledge OPTIMAL Structural Solutions LDA for the manufacturing of the panels, Smartec S.A. for the FOS procurement, and our colleagues from University of Patras for their technical support.

References

[1] E. J. Tuegel, A. R. Ingraffea, T. G. Eason, and S. M. Spottswood, "Reengineering Aircraft Structural Life Prediction Using a Digital Twin," *Int. J. Aerosp. Eng.*, vol. 2011, pp. 1–14, 2011.

[2] E. Tuegel, "The Airframe Digital Twin: Some Challenges to Realization," in *Structures, Structural Dynamics and Materials Conference 20th AIAA/ASME/AHS Adaptive Structures Conference 14th AIAA*, Apr. 2012.

[3] K. Reifsnider and P. Majumdar, "Multiphysics stimulated simulation digital twin methods for fleet management," in *54th AIAA/ASME/ASCE/AHS/ASC Structures, Structural Dynamics, and Materials Conference*, 2013.

[4] B. R. Seshadri and T. Krishnamurthy, "Structural health management of damaged aircraft structures using the digital twin concept," in *25th AIAA/AHS Adaptive Structures Conference*, 2013.

[5] E. M. Kraft, "The US air force digital thread/digital Twin – life cycle integration and use of computational and experimental knowledge," in *54th AIAA Aerospace Sciences Meeting*, 2016.

[6] M. Liao, G. Renaud, and Y. Bombardier, "Airframe digital twin technology adaptability assessment and technology demonstration," *Eng. Fract. Mech.*, vol. 225, 2020.

[7] E. Glaessgen and D. Stargel, "The Digital Twin Paradigm for Future NASA and U.S. Air Force Vehicles," in *53rd AIAA/ASME/ASCE/AHS/ASC Structures, Structural Dynamics and Materials Conference - Special Session on the Digital Twin*, Apr. 2012.

[8] H. Millwater, J. Ocampo, and N. Crosby, "Probabilistic methods for risk assessment of airframe digital twin structures," *Eng. Fract. Mech.*, vol. 221, 2019.

[9] P. E. Leser, J. E. Warner, W. P. Leser, G. F. Bomarito, J. A. Newman, and J. D. Hochhalter, "A digital twin feasibility study (Part II): Non-deterministic predictions of fatigue life using in-situ diagnostics and prognostics," *Eng. Fract. Mech.*, vol. 229, 2020.

[10] M. Grieves and J. Vickers, "Digital twin: Mitigating unpredictable, undesirable emergent behavior in complex systems," in Transdisciplinary Perspectives on Complex Systems: New Findings and Approaches, 2016.

[11] K. Worden, E. J. Cross, P. Gardner, R. J. Barthorpe, and D. J. Wagg, "On digital twins, mirrors and virtualisations," In: Barthorpe R. (eds) *Model Validation and Uncertainty Quantification*, Volume 3. Conference Proceedings of the Society for Experimental Mechanics Series. Springer, Cham. 2020.

[12] D. J. Wagg, K. Worden, R. J. Barthorpe, and P. Gardner, "Digital Twins: State-of-the-Art and Future Directions for Modeling and Simulation in Engineering Dynamics Applications," *ASCE-ASME J Risk Uncert Engrg Sys Part B Mech Engrg*, vol. 6, no. 3, Sep. 2020.

[13] P. E. Leser et al., "Probabilistic fatigue damage prognosis using surrogate models trained via three-dimensional finite element analysis," *Struct. Heal. Monit.*, vol. 16, no. 3, pp. 291–308, 2017.

[14] S. Chakraborty, S. Adhikari, and R. Ganguli, "The role of surrogate models in the development of digital twins of dynamic systems," *Appl. Math. Model.*, vol. 90, pp. 662–681, 2021.

[15] M. G. Kapteyn, D. J. Knezevic, D. B. P. Huynh, M. Tran, and K. E. Willcox, "Data-driven physics-based digital twins via a library of component-based reduced-order models," *Int. J. Numer. Methods Eng.*, 2020.

[16] T. G. Ritto and F. A. Rochinha, "Digital twin, physics-based model, and machine learning applied to damage detection in structures," *Mech. Syst. Signal Process.*, vol. 155, 2021.

[17] J. E. Warner, W. P. Leser, P. E. Leser, G. F. Bomarito, J. D. Hochhalter, and A. J. Newman, "A Computationally-Efficient Probabilistic Approach to Model-Based Damage Diagnosis," *Int. J. Progn. Heal. Manag.*, 2017.

[18] C. Li, S. Mahadevan, Y. Ling, S. Choze, and L. Wang, "Dynamic Bayesian network for aircraft wing health monitoring digital twin," *AIAA J.*, vol. 55, no. 3, pp. 930–941, 2017.

[19] P. Gardner, M. Dal Borgo, V. Ruffini, A. J. Hughes, Y. Zhu, and D. J. Wagg, "Towards the Development of an Operational Digital Twin," *Vibration*, vol. 3, no. 3, pp. 235–265, Sep. 2020.

[20] D. Cristiani, C. Sbarufatti, F. Cadini, and M. Giglio, "Fatigue damage diagnosis and prognosis of an aeronautical structure based on surrogate modelling and particle filter," *Struct. Heal. Monit.*, 2020, doi: 10.1177/1475921720971551.

[21] P. M. Karve, Y. Guo, B. Kapusuzoglu, S. Mahadevan, and M. A. Haile, "Digital twin approach for damage-tolerant mission planning under uncertainty," *Eng. Fract. Mech.*, vol. 225, 2020.

[22] Y. Ye, Q. Yang, F. Yang, Y. Huo, and S. Meng, "Digital twin for the structural health management of reusable spacecraft: A case study," *Eng. Fract. Mech.*, vol. 234, 2020.

[23] D. P. Milanoski and T. H. Loutas, "Strain-based health indicators for the structural health monitoring of stiffened composite panels," *J. Intell. Mater. Syst. Struct.*, vol. 32, no. 3, pp. 255–266, 2021, doi:10.1177/1045389X20924822

[24] D. Milanoski, G. Galanopoulos, A. Broer, D. Zarouchas, and T. Loutas, "A Strain-Based Health Indicator for the SHM of Skin-to-Stringer Disbond Growth of Composite Stiffened Panels in Fatigue," In: Rizzo P., Milazzo A. (eds) *European Workshop on Structural Health Monitoring. EWSHM 2020. Lecture Notes in Civil Engineering*, vol 127. Springer, Cham. 2021, pp. 626–635, doi:10.1007/978-3-030-64594-6_61

[25] S. G. Lekhnitskii, Anisotropic Plates. Gordon & Breach Science Publishers, New York 1968.

[26] K. O. Hill and G. Meltz, "Fiber Bragg grating technology fundamentals and overview," *J. Light. Technol.*, vol. 15, no. 8, pp. 1263–1276, 1997.

[27] R. Di Sante, "Fibre optic sensors for structural health monitoring of aircraft composite structures: Recent advances and applications," *Sensors (Switzerland)*, vol. 15, no. 8, pp. 18666–18713, 2015.

[28] A. Broer, G. Galanopoulos, R. Benedictus, T. Loutas, and D. Zarouchas, "Fusion-based damage diagnostics for stiffened composite panels," *Struct. Heal. Monit.*, 2021, doi:10.1177/14759217211007127.

[29] L. Grassia, M. Iannone, A. Califano, and A. D'Amore, "Strain based method for monitoring the health state of composite structures," *Compos. Part B Eng.*, vol. 176, 2019.

[30] A. I. J. Forrester, A. Sobester, and A. J. Keane, Engineering Design via Surrogate Modelling: A Practical Guide. Washington, DC: American Institute of Aeronautics and Astronautics, Inc., 2008.